

Finite Element Analysis of Electromagnetic Fields Emitted by Overhead High-Voltage Power Lines



Eduard Lunca, Bogdan Constantin Neagu, and Silviu Vornicu

Abstract The overhead high-voltage power lines (OHVPLs) are considered significant sources of extremely low frequency (ELF) electric and magnetic fields (EMFs), whose potential health effects became during the past decades a matter of scientific debate and public concern all over the world. In this chapter, a simple and yet effective finite element (FE) approach is proposed to compute and analyze—from the perspective of public exposure—both electric and magnetic fields emitted by typical configurations of OHVPLs belonging to the Romanian power grid. First, a 2D ANSYS Maxwell model is developed for the specific instance of a 110 kV double-circuit OHVPL and validated against two software tools based on quasi-static analytical methods, PowerELT and PowerMAG. Next, it will be used to investigate exposure to ELF-EMFs emitted by a selection of OHVPLs with nominal voltages of 110 kV, 220 kV and 400 kV, taking into consideration influencing factors such as loading, phasing and ground clearance. Compliance with the exposure guidelines specified by the International Commission on Non-Ionizing Radiation Protection (ICNIRP) for general public is assessed for each particular case. As a result, all calculated magnetic fields are below the ICNIRP limit of 100 μ T, while the electric fields exceed the ICNIRP limit of 5000 V/m only in limited areas beneath the 400 kV OHVPLs. The calculated field levels are in line with those reported in the scientific literature for similar OHVPLs.

E. Lunca (✉) · S. Vornicu

Department of Electrical Measurements and Materials, Gheorghe Asachi Technical University of Iasi, Iasi, Romania

e-mail: elunca@tuiasi.ro

S. Vornicu

e-mail: silviusieca@gmail.com

B. C. Neagu

Power System Department, Electrical Engineering Faculty, Gheorghe Asachi Technical University of Iasi, Iasi, Romania

e-mail: bogdan.neagu@tuiasi.ro

© The Author(s), under exclusive license to Springer Nature Switzerland AG 2021

795

N. Mahdavi Tabatabaei and N. Bizon (eds.), *Numerical Methods*

for Energy Applications, Power Systems,

https://doi.org/10.1007/978-3-030-62191-9_29

Keywords Overhead high-voltage power line · Electric field · Magnetic field · Public exposure · 2D ANSYS maxwell model

Abbreviations

A. Acronyms

2D	Two-Dimensional
ACSR	Aluminum Conductor Steel-Reinforced
ELF	Extremely Low Frequency
EMF	Electric and Magnetic Fields
EU	European Union
FE	Finite Element
FEM	Finite Element Method
IARC	International Agency for Research on Cancer
ICNIRP	International Commission on Non-Ionizing Radiation Protection
IEEE	Institute of Electrical and Electronics Engineers
OHVPL	Overhead High-Voltage Power Line
RMS	Root Mean Square
SW	Shield Wire
T	Transposed
U	Untransposed
WHO	World Health Organization

B. Symbols/Parameters

B	Magnetic flux density
E	Electric field strength
i	Conductor number
I_i	Phase current of conductor i
U_i	Phase voltage of conductor i
d_i	Lateral distance from centerline to conductor i
h_i	Height of conductor i
h_g	Line-to-ground clearance
h	Calculation height above ground
R_{eq}	Bundle conductor equivalent radius

1 General

The electricity has many benefits in our daily life. But generating, transmitting, distributing and using electricity can expose people to ELF-EMFs, which interact with the human body by mainly inducing electric currents in it. During the past

decades, a lot of research has been devoted to investigation of possible health effects of exposure to ELF-EMFs, including childhood and adult cancers, reproductive dysfunctions, cardiovascular and developmental disorders, immunological modifications, neurological effects, etc. Particularly, a (poor) statistical link between childhood leukemia and prolonged exposure to residential ELF magnetic fields higher than 0.3–0.4 μT has been reported by a number of epidemiological studies [1, 2]. In 2002, based on these findings, the International Agency for Research on Cancer (IARC)—an intergovernmental agency activating within the World Health Organization (WHO)—has concluded that the ELF magnetic fields are “possibly carcinogenic to humans” (Group 2B carcinogens, designating agents for which the evidence in humans is limited and the evidence in animals is “less than sufficient”). As for ELF electric fields, IARC has concluded that they are “unclassifiable as to carcinogenicity in humans” (Group 3 carcinogens) [3].

Aiming at preventing the established health effects associated with short-term exposure to high intensity ELF-EMFs, principally induced currents, ICNIRP and IEEE (the Institute of Electrical and Electronics Engineers) have formulated exposure guidelines in 1998 [4] and 2002 [5], respectively. According to the scientific information currently available, long-term exposure to ELF field levels not exceeding the limits prescribed by these guidelines is considered safe for the purpose of protecting human health. There is no established evidence that exposure to ELF-EMFs emitted by power lines, substations, transformers or other electrical equipment, regardless of the proximity, can cause any known health effects. But there is a continuous debate as to what might be adequate precautionary approaches at these lower field levels. Furthermore, the general public often expresses concern about ELF-EMFs, especially in relation with setting up new overhead high-voltage power lines or living in their vicinity [6–9].

The OHVPLs are considered significant sources of both electric and magnetic fields. Both fields are strongest directly under the OHVPL and sharply reduce with distance from it. Of course, in addition to distance, there are many other factors influencing the ELF-EMFs originating from OHVPLs, including voltage, current, phasing, ground clearance, observation height above the ground, balance within circuit, balance between circuits, conductor bundle, existence of parallel lines, ground resistivity (conductivity), etc. Moreover, the electric fields are greatly attenuated by buildings, walls, fences, trees and other obstacles in the neighborhood, but the magnetic fields pass through most materials and cannot be attenuated as easily as the electric fields [10–12].

To determine ELF electric and magnetic field levels emitted by OHVPLs and to assess compliance with relevant exposure limits, both measurements and computations can be performed [13–19]. Computations are often preferable to measurements because they can be conducted for any desired exposure scenario rather than being confined to the particular conditions at the time of taking measurements. Analytical and numerical methods can be used for computations, usually employing two-dimensional (2D) models because of their simplicity [20–33]. Very often, the numerical calculations (simulations) exploit the finite element method (FEM), which is

recognized for its ability to generate accurate 2D electric and magnetic field distributions in the transverse section of the OHVPLs and of other power–frequency systems [19, 29–33].

In this chapter, a simple and yet effective FEM approach is proposed to compute and analyze—from the perspective of public exposure—ELF electric and magnetic fields produced by typical configurations of OHVPLs belonging to the Romanian power grid. Computations are performed with ANSYS Maxwell 2D electromagnetic simulation software, mainly in the form of RMS electric field strength and RMS magnetic flux density lateral profiles, at the standard height $h = 1$ m above the ground level. It is worthwhile to remark that Romania, as a member of the European Union (EU), has implemented exposure limits derived from the *Council Recommendation of 12 July 1999 on the limitation of exposure of the general public to electromagnetic fields (0 Hz–300 GHz)* [34], which is based on the guidelines issued by ICNIRP in 1998. For power–frequency electric and magnetic fields, these limits are 5000 V/m and 100 μ T, respectively.

From this point, the chapter is organized as follows. First, a 2D ANSYS Maxwell model for computing ELF electric and magnetic fields around OHVPLs will be developed and validated against simulation software based on analytical methods. Next, it will be used to investigate exposure to ELF-EMFs generated by a selection of OHVPLs with nominal voltages of 110, 220 and 400 kV. As already mentioned, special attention will be given to the field distribution at 1 m height above the ground, taking into consideration influencing factors such as loading, phasing and ground clearance. Compliance with the ICNIRP exposure limits for general public will be assessed for each particular case.

2 2D ANSYS Maxwell Model for Computing ELF Electric and Magnetic Fields Around OHVPLs

ANSYS Maxwell 2D is a high-performance low frequency electromagnetic field simulation software that uses the finite element method for solving electric, magnetostatic, eddy current and transient problems. Therefore, it may serve as an appropriate tool for computing exposure to ELF-EMFs originating from OHVPLs, but such investigations are rather rare and mostly focused only on the magnetic field exposure [17, 35, 36]. As an extension of a recent study by the authors [11], this section presents the development and validation of a 2D Maxwell model for computing both electric and magnetic fields emitted by various OHVPLs. The model is implemented for a common configuration of 110 kV double-circuit line used for primary power distribution, but it can easily be applied to any other OHVPL. The model validation is achieved against previously developed software based on quasi-static analytical methods.

2.1 Model Development

The 110 kV double-circuit OHVPL selected for model implementation—often found in the proximity of urban settings—has geometry dictated by suspension towers of Sn 110.252 type, as illustrated in Fig. 1. The phases of the two circuits are realized with Aluminum Conductor Steel-Reinforced (ACSR) cables of Sect. 240/40 mm² (21.7 mm exterior diameter), while the shield wire (SW) is represented by a 160/95 mm² ACSR conductor (20.75 mm exterior diameter). The OHVPL is considered to operate at a load of 500 A (close to the maximum rated current), with the phases of the two circuits perfectly balanced. In addition, because the field level largely depends on the relative phasing between the two circuits, we assumed both untransposed (ABC/A'B'C') and directly transposed (ABC/C'B'A') phase arrangements, which

Fig. 1 Suspension tower of Sn 110.252 type (dimensions are given in mm)

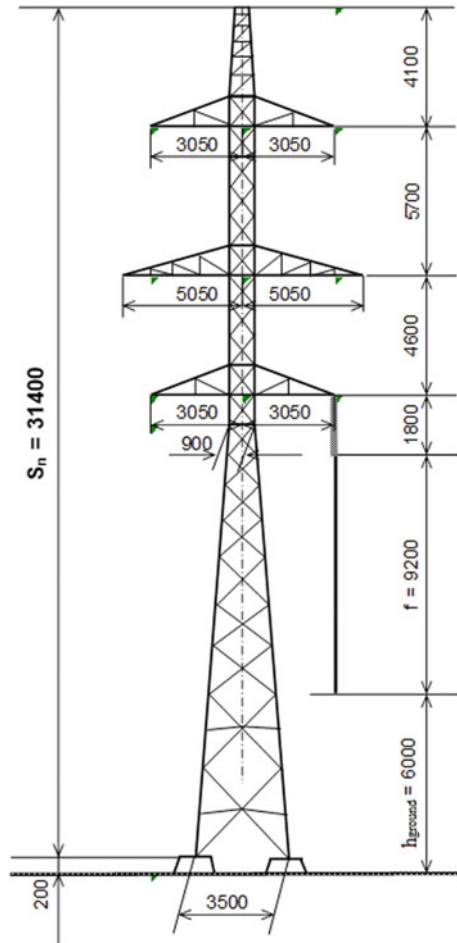
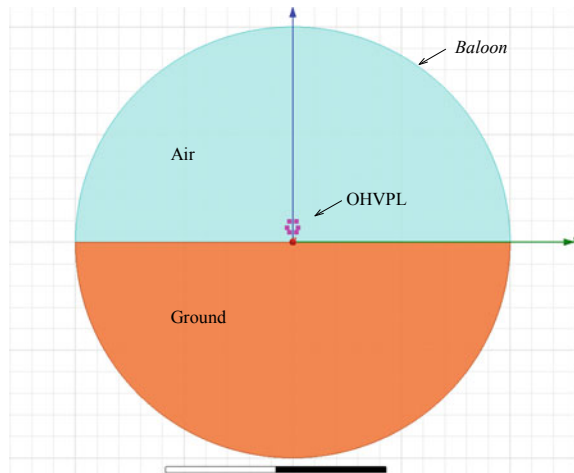


Fig. 2 Global FEM geometric model of the 110 kV double-circuit OHVPL



clearly determine the maximum and minimum exposure to the sides of the line [37, 38], where people are most likely to live or spend time.

a. FEM geometric model

The global FEM geometric model is presented in Fig. 2, where the considered 110 kV double-circuit OHVPL is placed above a ground with the electrical conductivity of 0.01 S/m, the relative electric permittivity of 10 and the relative magnetic permeability of 1. The ground clearance, namely 9 m, corresponds to an “average height” of the OHVPL above the ground, calculated as $h_{\text{avg}} = h_{\text{max}} - (2/3) \cdot f$ [39], where $h_{\text{max}} = 15.2$ m represents the maximum height of the conductors (at tower) and $f = 9.2$ m is the conductors sag. The active conductors are modeled as presented in Fig. 3, as simple aluminum cylinders with the electrical conductivity of $3.8 \cdot 10^7$ S/m, the relative electric permittivity of 1 and the relative magnetic permeability of 1, while the influence of the SW on the electric and magnetic field distribution is ignored (the SW is not included in simulation). The applied boundary conditions are of Balloon type, which models the region outside the defined space as extending to infinity. The radius of the bounded region is taken $R = 200$ m, sufficiently large to determine the behavior of the two fields well outside the power line corridor, even for OHVPLs with higher nominal voltages. All simulations conducted in this study assume a total number of mesh elements of 1,223,286, but it can be lowered for more rapid and yet satisfactory analyzes.

b. Magnetic field calculation

The magnetic field distribution around the OHVPL is obtained using the *eddy current solver*, which allows calculating magnetic fields that oscillate with a frequency (in this case, 50 Hz). However, because the magnetic field distributions generated with this solver are reported in terms of instantaneous magnetic flux density values over a 20 ms period, further post-processing is necessary to generate RMS

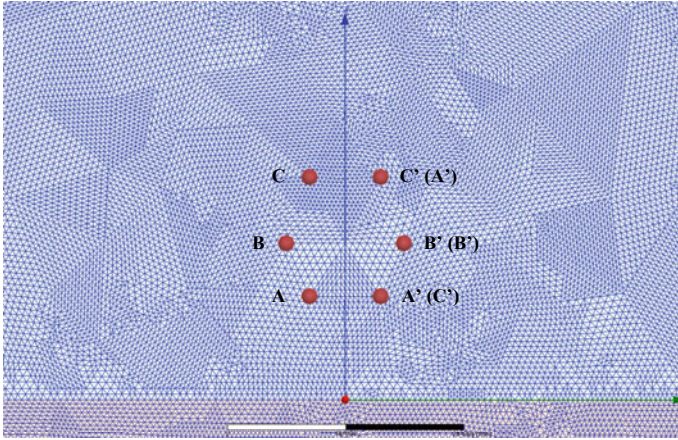


Fig. 3 Discretized OHVPL region

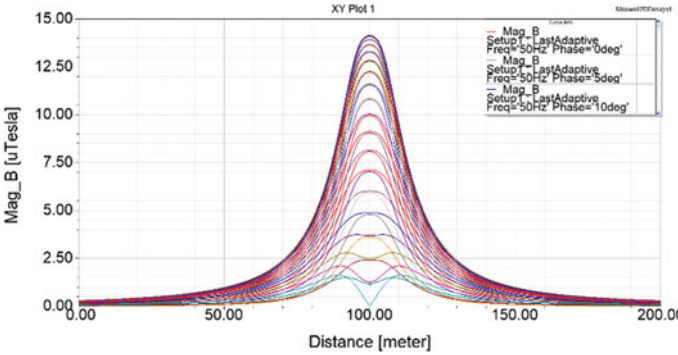


Fig. 4 Instantaneous magnetic flux density profiles at $h = 1$ m, for U phasing

magnetic flux density (lateral) profiles at the height $h = 1$ m, as often used for assessing exposure to ELF-EMFs from overhead power lines. Consequently, multiple instantaneous magnetic flux density profiles have been imported into Microsoft Excel, where they have been processed in a point-by-point fashion, according to the formula [11]:

$$B_{RMS}(i) = \sqrt{\frac{1}{N} \sum_{n=1}^N B_n^2(i)}, \tag{1}$$

where $B_1(i), \dots, B_N(i)$ represent the instantaneous values of the magnetic flux density corresponding to the point i of the profile and $N = 73$ is the total number of values.

Figure 4 presents instantaneous magnetic flux density profiles obtained for untransposed (U) phasing, while Fig. 5 shows similar profiles obtained for transposed (T) phasing. The correspondent RMS magnetic flux density profiles—computed with Eq. (1)—are comparatively presented in Fig. 6. Starting at a certain distance from the centerline, any other phase arrangement will generate an RMS magnetic flux density profile between these two limit plots.

Figures 7 and 8 illustrate the magnetic field distribution around the OHVPL at the time instants corresponding to the maximum field profiles in Figs. 4 and 5, respectively. As evident, an extra degree of cancellation between the magnetic fields generated by the two circuits can be observed for transposed phasing. The distance from the centerline is 30 m in both distributions.

c. Electric field calculation

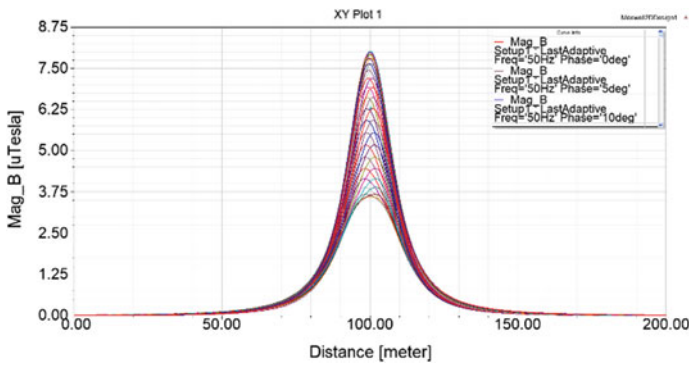


Fig. 5 Instantaneous magnetic flux density profiles at $h = 1$ m, for T phasing

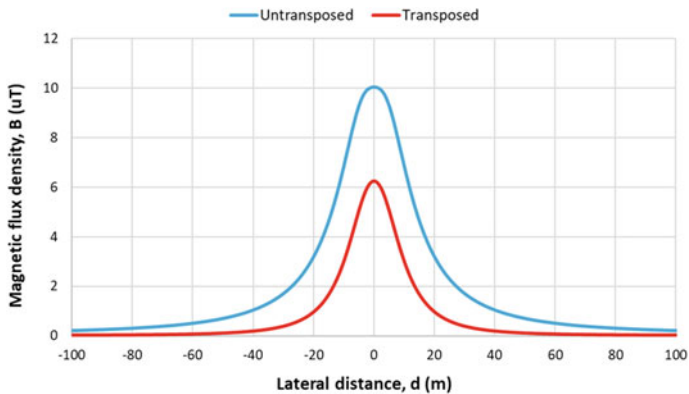


Fig. 6 Comparison between RMS magnetic flux density profiles obtained for untransposed and transposed phasing

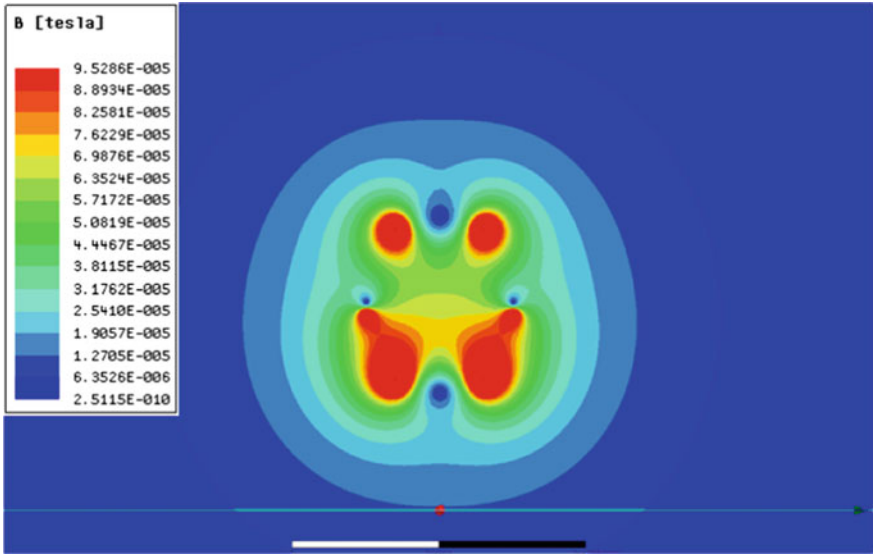


Fig. 7 The magnetic field distribution around the 110 kV double-circuit OHVPL for U phasing ($t = 10.83$ ms)

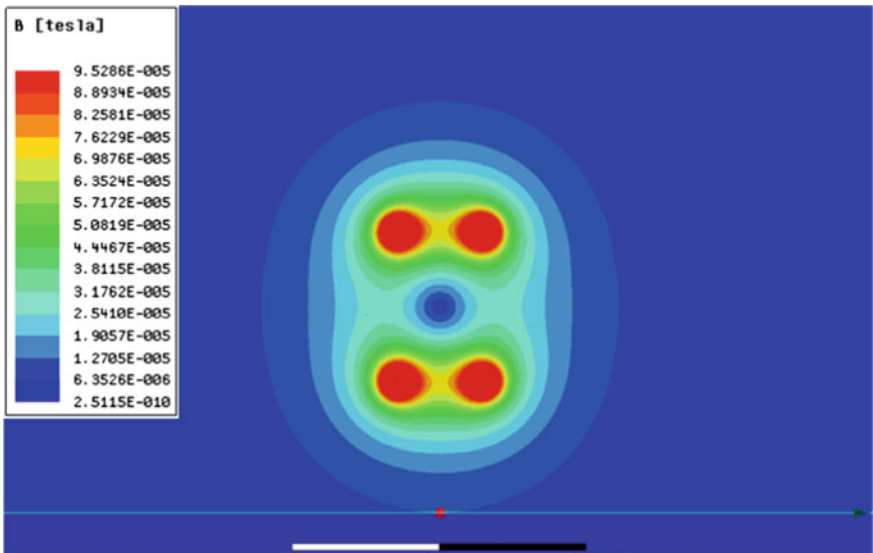


Fig. 8 The magnetic field distribution around the 110 kV double-circuit OHVPL for T phasing ($t = 11.66$ ms)

The electric field distribution around the OHVPL is determined using the *AC conduction solver*, which allows calculating sinusoidally-varying electric fields (here, varying at 50 Hz). And this time, to generate RMS electric field strength lateral profiles at the height $h = 1$ m, multiple profiles of instantaneous electric field strength have been imported into Microsoft Excel, where they have been processed in the same way, by applying the formula [11]:

$$E_{RMS}(i) = \sqrt{\frac{1}{N} \sum_{n=1}^N E_n^2(i)} \tag{2}$$

where $E_1(i), \dots, E_N(i)$ represent the instantaneous values of the electric field strength corresponding to the point i of the profile and $N = 73$ is the total number of values.

As in the case of magnetic field, Fig. 9 gives instantaneous electric field strength profiles obtained for U phasing, while Fig. 10 shows profiles obtained for T phasing. The two associated RMS electric field strength profiles—computed with Eq. (2)—are compared in Fig. 11.

Figures 12 and 13 illustrate the momentary distribution of the electric field around the OHVPL corresponding to the maximum field profiles in Figs. 9 and 10, respectively. Once again, an extra degree of cancellation between the electric fields generated by the two circuits can be observed for transposed phasing. As in the case of magnetic field, the distance from the centerline is 30 m in both distributions.

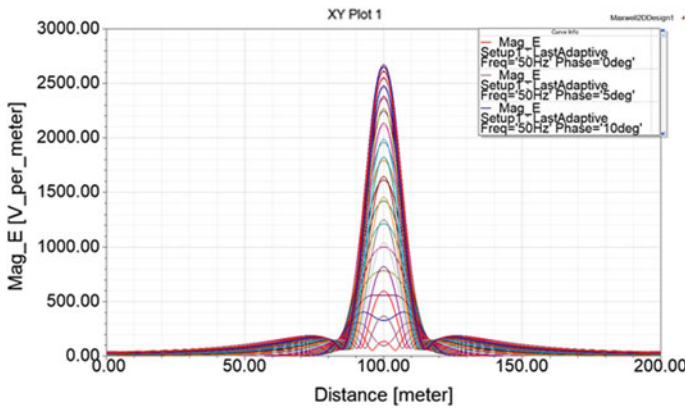


Fig. 9 Instantaneous electric field strength profiles at $h = 1$ m, for U phasing

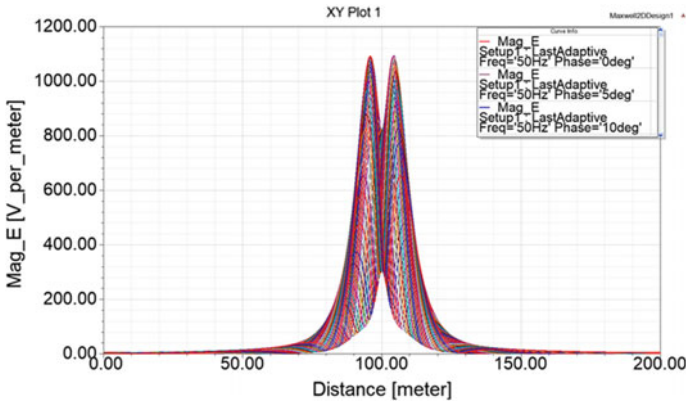


Fig. 10 Instantaneous electric field strength profiles at $h = 1$ m, for T phasing

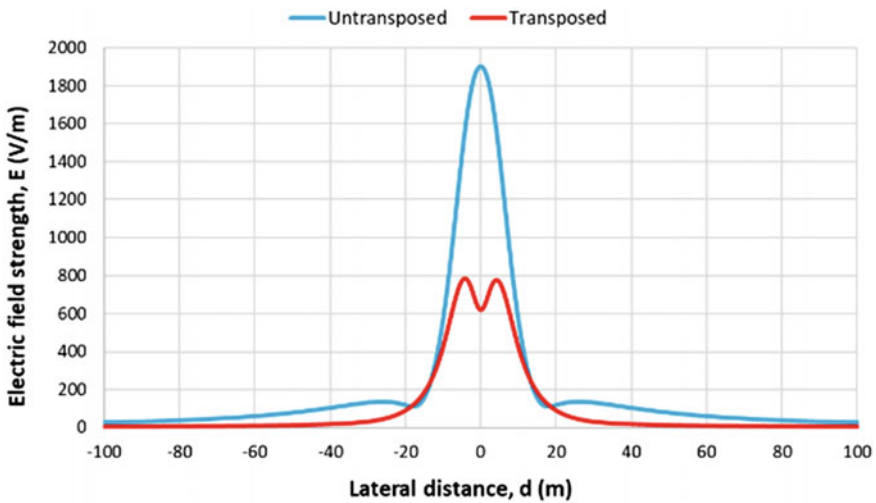


Fig. 11 Comparison between RMS electric field strength profiles obtained for untransposed and transposed phasing

2.2 Model Validation

The model validation has mainly been performed with the help of two interactive software tools based on analytical methods, *PowerELT* and *PowerMAG* [28], which are capable to produce accurate electric and magnetic field (lateral) profiles at any user-defined height above the ground level, together with 2D electric and magnetic field distributions in the transverse section of the OHVPL, in any rectangular plotting area also defined by user. Assuming the same power line geometry, and voltage and current information (amplitude and phase, respectively), Fig. 14 compares RMS

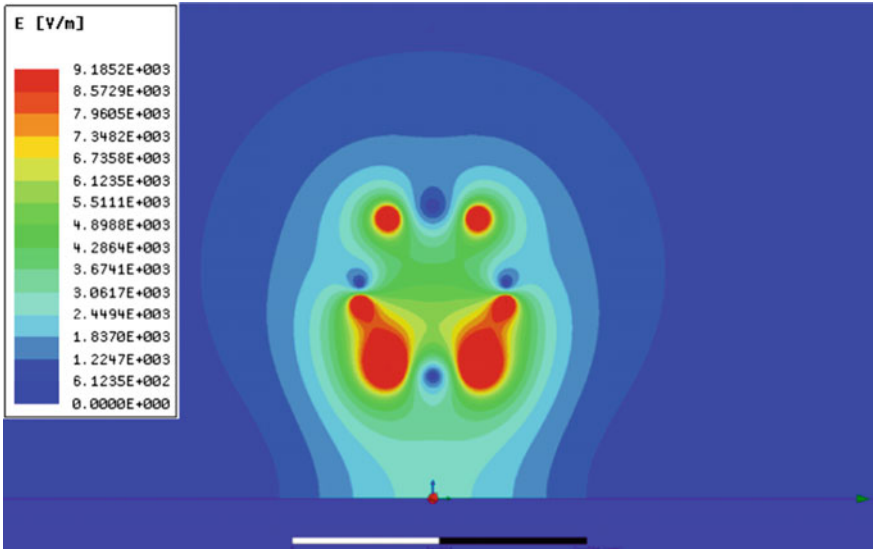


Fig. 12 The electric field strength distribution around the 110 kV OHVPL for U phasing ($t = 10.55$ ms)

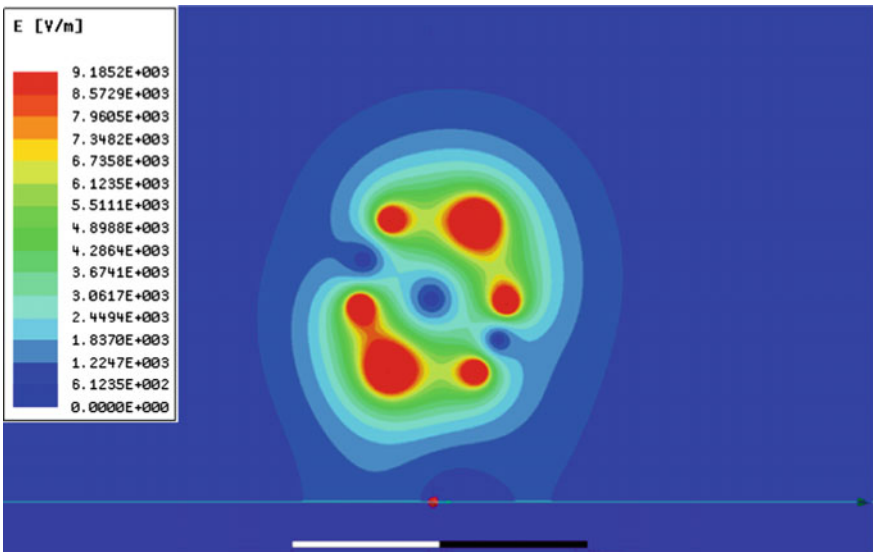


Fig. 13 The electric field strength distribution around the 110 kV OHVPL for T phasing ($t = 20$ ms)

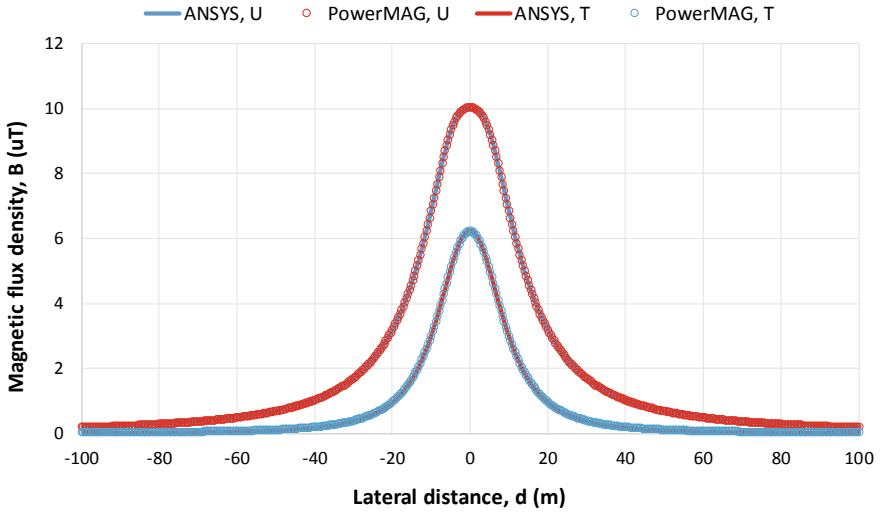


Fig. 14 Comparison between RMS magnetic flux density profiles obtained by numerical simulation and analytical computation

magnetic flux density profiles computed with the developed 2D ANSYS Maxwell model and PowerMAG software. Similarly, Fig. 15 compares RMS electric field strength profiles computed with the developed 2D ANSYS Maxwell model and

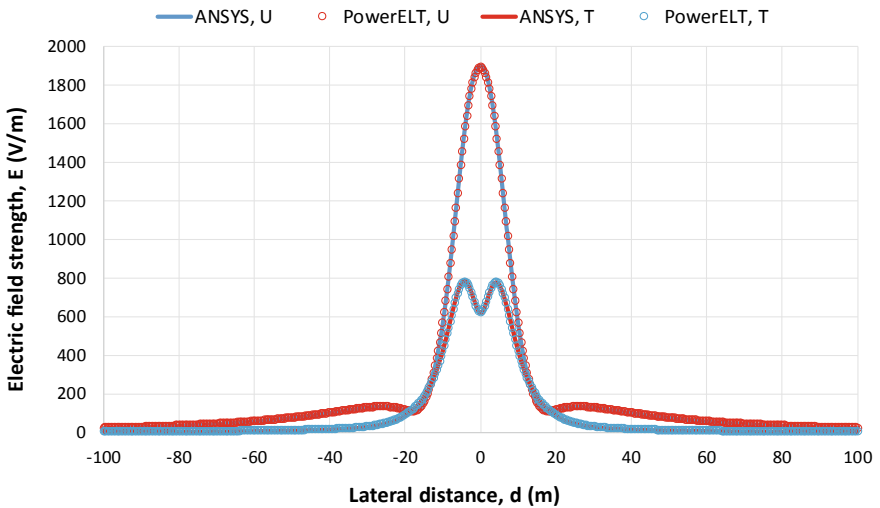


Fig. 15 Comparison between RMS electric field strength profiles obtained by numerical simulation and analytical computation

PowerELT software. As obvious, there is an excellent agreement between numerical and analytical results, regardless the phasing (U or T).

Similar comparisons have also been made for OHVPLs with higher nominal voltages (i.e., larger physical dimensions), each time obtaining perfect matching between simulated profiles. Exposure to ELF-EMFs from some of these lines, under various conditions, will be discussed in the subsequent section.

3 Finite Element Analysis of ELF-EMFs from Typical OHVPLs Used in the Romanian Power Grid

In Romania, OHVPLs are used for both power transmission and power distribution. Power transmission is achieved through a total length of 8759.4 km of OHVPLs, of which [40]: 3.1 km—750 kV, 4915.2 km—400 kV, 3875.6 km—220 kV and 40.4 km—110 kV, where 482.6 km serves as interconnection lines. In addition, power distribution operators make use of more than 20,000 km of OHVPLs operating at 110 kV. Thus, for assessing exposure to ELF-EMFs emitted by these OHVPLs, we have selected two double-circuit lines with nominal voltages of 110 kV and 220 kV, respectively, and a single-circuit line with nominal voltage of 400 kV, which can be considered typical. Finite element analysis of ELF-EMFs from these lines assumes the same conditions as in the described model, except that computations will be performed for three different ground clearances (minimum, average and maximum), as well as for maximum allowable current. However, because of the direct proportionality between current and magnetic flux density, the computed fields can easily be scaled down for more common loads.

3.1 ELF-EMFs from the 110 kV Double-Circuit OHVPL

In essence, the 110 kV double-circuit OHVPL subjected to investigations is the same used for model development, which has geometry dictated by suspension towers of Sn 110.252 type. As already mentioned, the two circuits are realized with standard 240/40 mm² ACSR conductors (21.7 mm exterior diameter), which have a maximum allowable current of 575 A (RMS). All other input data for this line are presented in Table 1, where d_i is the lateral distance from the OHVPL centerline to the conductor i , h_i represents the height of the conductor i and h_g denotes the ground clearance of the line: 6 m, 9 m and 15.2 m, respectively.

a. Magnetic field distribution

Figure 16 presents RMS magnetic flux density profiles at the height $h = 1$ m, for untransposed phasing. The maximum magnetic field beneath the line (not necessarily at the centerline) varies from 5.48 μ T for $h_g = 15.2$ m (at tower) to 18.5 μ T for $h_g = 6$ m (at mid-span), which is generally below 18.5% of the ICNIRP limit for

Table 1 Input data for the 110 kV double-circuit OHVPL using towers of Sn 110.252 type (untransposed phasing)

Phase conductor	i	d_i [m]	h_i [m]	\underline{U}_i [kV]	\underline{I}_i [A]
A	1	-3.05	h_g	$63.51 \angle 0^\circ$	$575 \angle 0^\circ$
B	2	-5.05	$h_g + 4.6$	$63.51 \angle -120^\circ$	$575 \angle -120^\circ$
C	3	-3.05	$h_g + 10.3$	$63.51 \angle 120^\circ$	$575 \angle 120^\circ$
A'	4	3.05	h_g	$63.51 \angle 0^\circ$	$575 \angle 0^\circ$
B'	5	5.05	$h_g + 4.6$	$63.51 \angle -120^\circ$	$575 \angle -120^\circ$
C'	6	3.05	$h_g + 10.3$	$63.51 \angle 120^\circ$	$575 \angle 120^\circ$

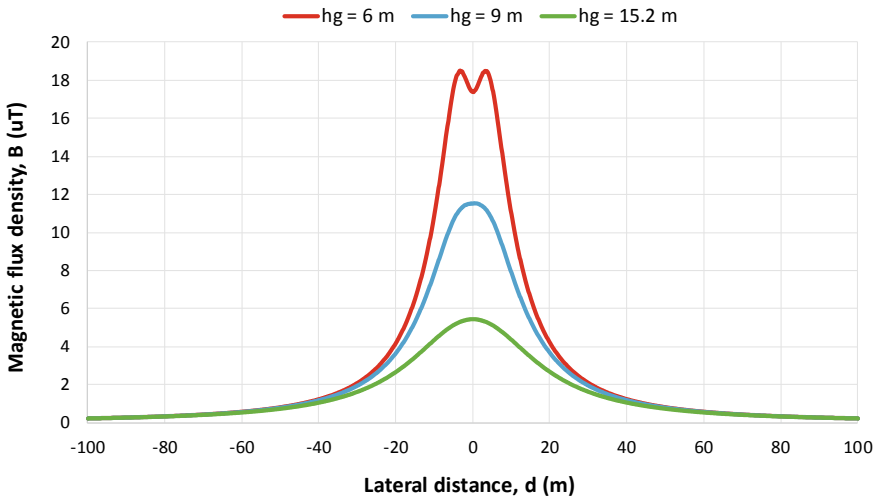


Fig. 16 RMS magnetic flux density profiles for the 110 kV OHVPL, for untransposed phasing and various ground clearances

general public, 100 μT . For transposed phasing (Fig. 17), the maximum magnetic field beneath the line varies from 2.12 μT for $h_g = 15.2$ m to 16.1 μT for $h_g = 6$ m, hence not exceeding 16.1% of the ICNIRP exposure limit. As it can easily be observed, starting with some distance from the centerline, the transposed phasing produces much lower magnetic field levels.

Considering the average clearance $h_g = 9$ m and a (more) typical loading of 325 A, Table 2 gives magnetic field levels at various distances from the centerline. Beneath the line, the magnetic flux density does not exceed 6.51 μT for U phasing and 4.03 μT for T phasing, while at the edge of the OHVPL corridor—18.5 m from the centerline, according to national regulations [41]—it decreases to 2.32 μT and 0.73 μT , respectively. The critical value of 0.4 μT —often used in epidemiological studies—is reached at a lateral distance of about 53.9 m and 24.5 m, respectively.

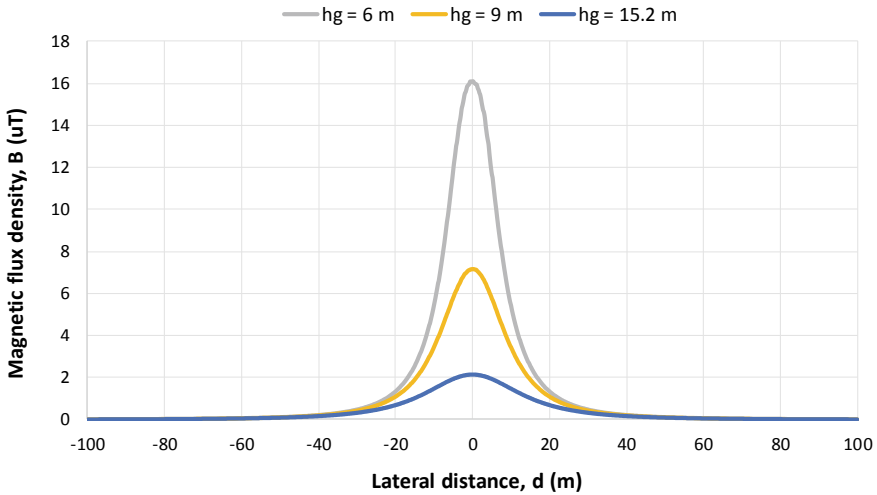


Fig. 17 RMS magnetic flux density profiles for the 110 kV OHVPL, for transposed phasing and various ground clearances

Table 2 Typical magnetic field levels from the 110 kV OHVPL ($h_g = 9\text{ m}$, $I = 325\text{ A}$)

Phasing	B [μT], at various lateral distances				
	<i>Maximum beneath line</i>	<i>18.5 m</i>	<i>25 m</i>	<i>50 m</i>	<i>100 m</i>
U	6.51	2.32	1.49	0.46	0.14
T	4.03	0.73	0.38	0.067	0.011

b. Electric field distribution

The RMS electric field strength distribution at the height $h = 1\text{ m}$ —for untransposed phasing—is illustrated in Fig. 18. The maximum electric field beneath the line (at the centerline) varies from 882.8 V/m at tower to 3017.2 V/m at mid-span, which is generally below 60.34% of the ICNIRP exposure limit for general public, 5000 V/m. For transposed phasing (Fig. 19), the maximum electric field levels beneath the line range from 243.2 V/m at tower to 1790.2 V/m at mid-span, hence not exceeding 35.8% of the exposure limit.

For the average clearance $h_g = 9\text{ m}$ (Table 3), the electric field strength beneath the line reaches 1901.8 V/m for U phasing and 784.4 V/m for T phasing, while the electric field strength at the corridor edge reaches 110.3 V/m and 109.5 V/m, respectively. At the distance of 50 m from the centerline route, the electric field levels fall to only 77 and 11.3 V/m, respectively, similar to the lowest levels measured at 30 cm distance from household appliances.

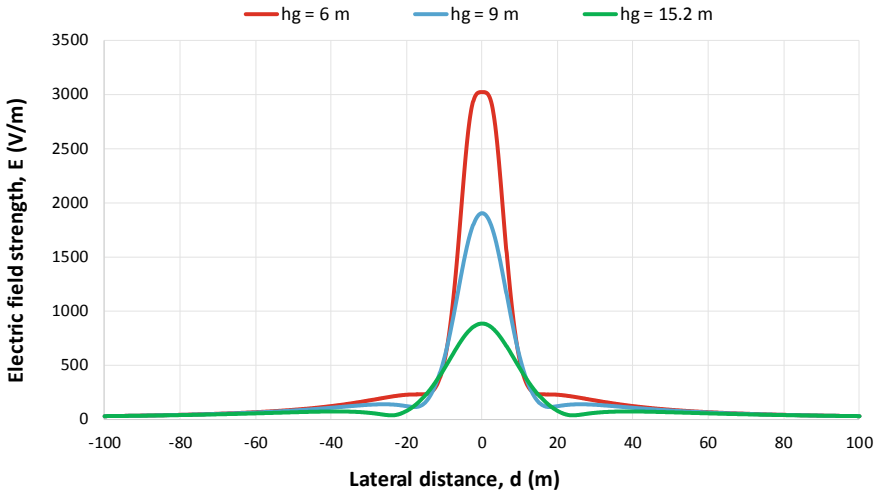


Fig. 18 RMS electric field strength profiles for the 110 kV OHVPL, for untransposed phasing and various ground clearances

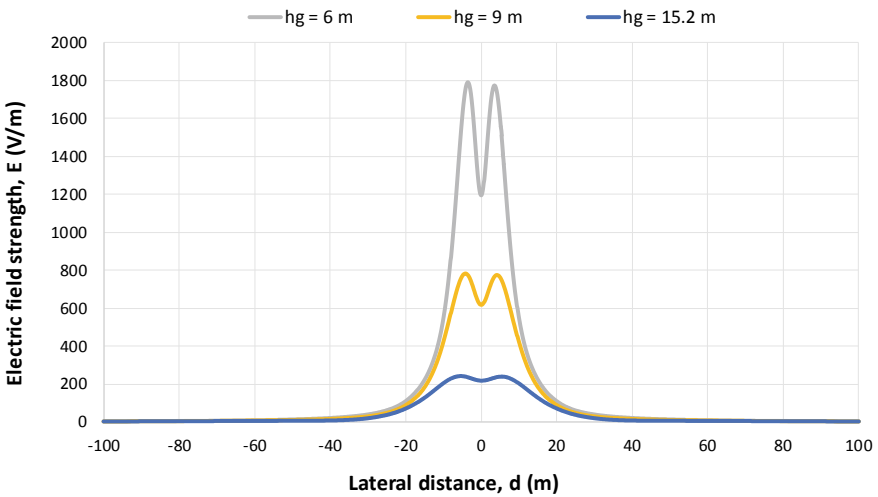


Fig. 19 RMS electric field strength profiles for the 110 kV OHVPL, for transposed phasing and various ground clearances

Table 3 Typical electric field levels from the 110 kV OHVPL ($h_g = 9\text{ m}$)

Phasing	E [V/m], at various lateral distances				
	<i>Maximum beneath line</i>	<i>18.5 m</i>	<i>25 m</i>	<i>50 m</i>	<i>100 m</i>
U	1901.8	110.3	134.4	77	25
T	784.4	109.5	47.9	11.3	3.3

3.2 ELF-EMFs from the 220 kV Double-Circuit OHVPL

The 220 kV double-circuit OHVPL selected for FE analysis has geometry dictated by suspension towers of Sn 220.202 type. The line is equipped with standard 450/75 mm² ACSR conductors (29.25 mm exterior diameter), for which the maximum allowable current is 975 A. Table 4 presents the geometrical data, as well as the voltage and current information used for computation, where the ground clearance h_g is taken 7 m, 11 m and 19 m, respectively. Because the geometry of this line is quite similar to the geometry of the 110 kV line, we expect similar electric and magnetic field distributions.

a. Magnetic field distribution

For untransposed phasing (Fig. 20), the maximum RMS magnetic flux density beneath the 220 kV OHVPL ranges from 7 μ T at tower to 23.9 μ T at mid-span, generally accounting for less than 24% of the ICNIRP exposure limit for general public. For transposed phasing (Fig. 21), the maximum RMS magnetic flux density along the half-span varies between 3.62 and 24.33 μ T, hence not exceeding 24.4% of the ICNIRP exposure limit. And this time, much lower field levels can be observed at larger distances from the line for T phasing.

Table 5 gives magnetic field levels at various distances from the OHVPL centerline for the average clearance $h_g = 11$ m and a (more usual) loading of 200 A. Beneath the line, the magnetic flux density does not exceed 2.87 μ T for U phasing and 2.35 μ T for T phasing, while at the edge of the OHVPL corridor—27.5 m from the centerline [41]—it decreases to 0.93 μ T and 0.42 μ T, respectively. The critical value of 0.4 μ T is reached at a lateral distance of about 45 m and 25.4 m, respectively. As we can see, because of the low load conditions, the typical exposure levels from this line are lower than those associated with the 110 kV OHVPL.

b. Electric field distribution

The electric field strength distribution for untransposed phasing is illustrated in Fig. 22. Beneath the 220 kV double-circuit OHVPL, the maximum field strength at the standard height $h = 1$ m ranges from 1452.8 V/m for $h_g = 19$ m to 4673.7 V/m for $h_g = 7$ m, which is very close to the ICNIRP limit for general public (93.5% of

Table 4 Input data for the 220 kV double-circuit OHVPL using towers of Sn 220.202 type (untransposed phasing)

Phase conductor	i	d_i [m]	h_i [m]	\underline{U}_i [kV]	\underline{I}_i [A]
A	1	-5.00	h_g	$127 \angle 0^\circ$	$975 \angle 0^\circ$
B	2	-8.00	$h_g + 6.5$	$127 \angle -120^\circ$	$975 \angle -120^\circ$
C	3	-5.00	$h_g + 13$	$127 \angle 120^\circ$	$975 \angle 120^\circ$
A'	4	5.00	h_g	$127 \angle 0^\circ$	$975 \angle 0^\circ$
B'	5	8.00	$h_g + 6.5$	$127 \angle -120^\circ$	$975 \angle -120^\circ$
C'	6	5.00	$h_g + 13$	$127 \angle 120^\circ$	$975 \angle 120^\circ$

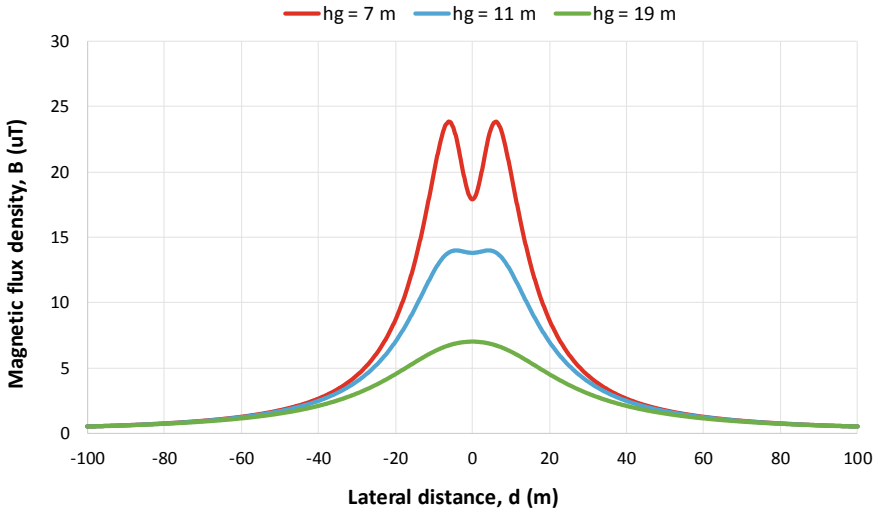


Fig. 20 RMS mag-netic flux density profiles for the 220 kV OHVPL, for untransposed phasing and various ground clearances

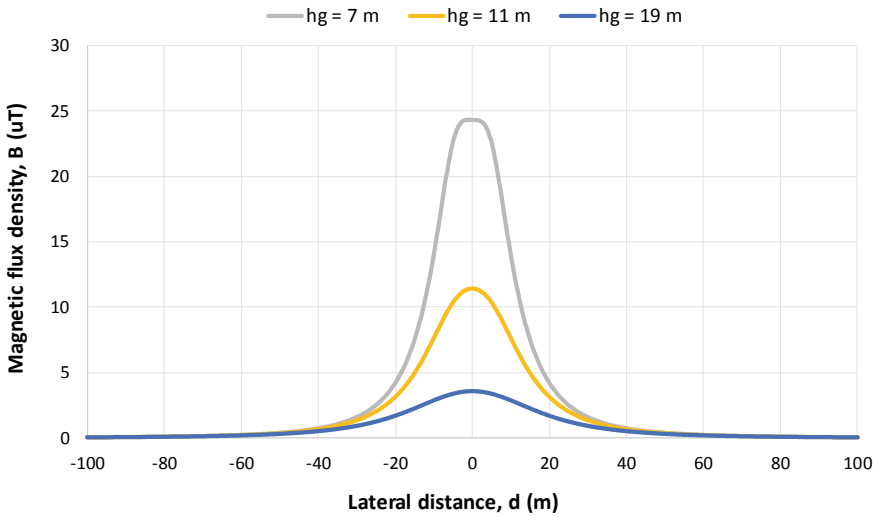


Fig. 21 RMS mag-netic flux density profiles for the 220 kV OHVPL, for transposed phasing and various ground clearances

Table 5 Typical magnetic field levels from the 220 kV OHVPL ($h_g = 11\text{ m}$, $I = 200\text{ A}$)

Phasing	B [μT], at various lateral distances				
	Maximum beneath line	25 m	27.5 m	50 m	100 m
U	2.87	1.07	0.93	0.35	0.11
T	2.35	0.42	0.34	0.076	0.01

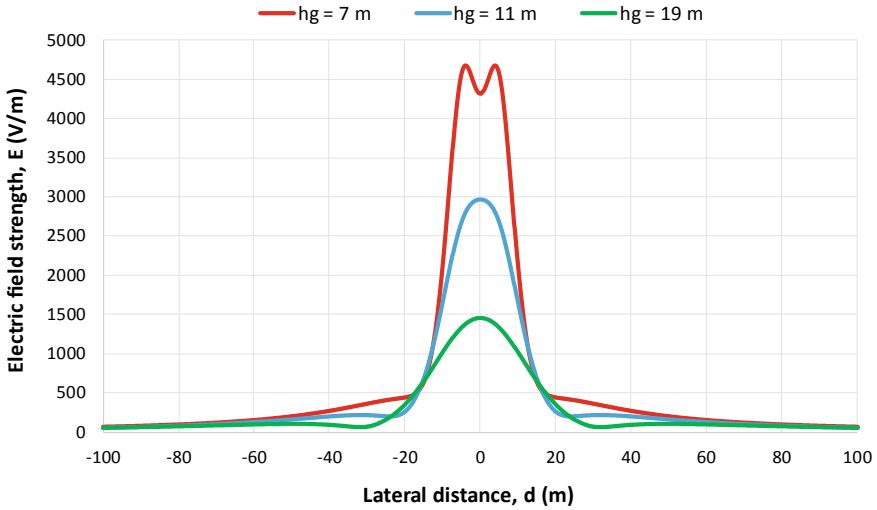


Fig. 22 RMS electric field strength profiles for the 220 kV OHVPL, for untransposed phasing and various ground clearances

the limit). For transposed phasing (Fig. 23), the maximum electric field strength at the same height lies in the range from 499.2 to 3653.9 V/m, which is below 73.1% of the ICNIRP exposure limit.

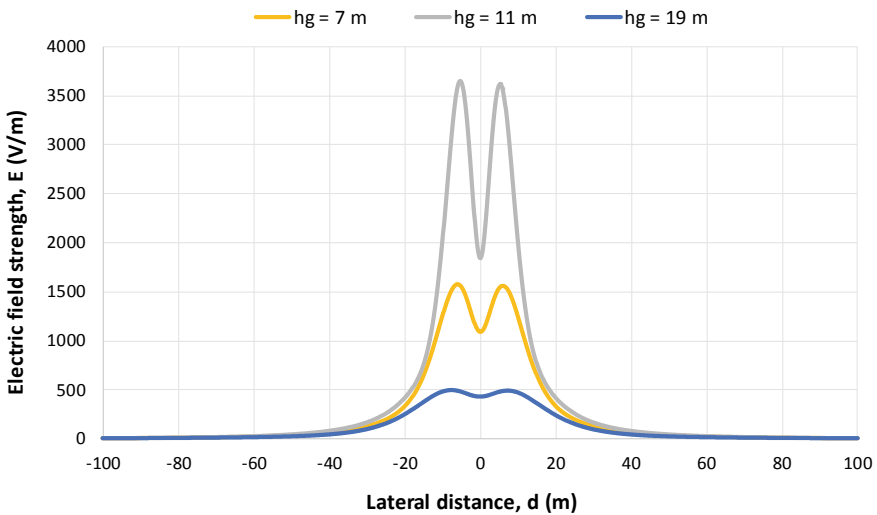


Fig. 23 RMS electric field strength profiles for the 220 kV OHVPL, for transposed phasing and various ground clearances

Table 6 Typical electric field levels from the 220 kV OHVPL ($h_g = 11$ m)

Phasing	E [V/m], at various lateral distances				
	<i>Maximum beneath line</i>	25 m	27.5 m	50 m	100 m
U	2969.5	207.6	215.9	161.7	60.5
T	1580	199	160	40	7.5

For the average clearance $h_g = 11$ m (Table 6), the electric field strength beneath the line reaches 2969.5 V/m for U phasing and 1580 V/m for T phasing, while the electric field strength at the corridor edge (27.5 m from the centerline) only reaches 215.9 V/m and 160 V/m, respectively. At 50 m from the OHVPL centerline, the electric field strength diminishes to 167.1 V/m and 40 V/m, respectively. As in the case of the 110 kV single-circuit OHVPL, such levels can also be measured at a distance of 30 cm from household appliances.

3.3 ELF-EMFs from the 400 kV Single-Circuit OHVPL

The last OHVPL selected for FE analysis is a 400 kV single-circuit line with geometry dictated by anchor portal towers of PAS 400.102 type. The line is equipped with two standard 450/75 mm² ACSR conductors per phase, with a distance between individual conductors of 0.4 m. The input data for this line are presented in Table 7, where the ground clearance h_g is taken 8.2 m, 12.6 m and 21.4 m, respectively. Magnetic field computations assume a maximum current of 1950 A.

a. Magnetic field distribution

The RMS magnetic flux density distribution at the height $h = 1$ m is illustrated in Fig. 24. As with the other investigated OHVPLs, the magnetic field beneath the 400 kV line does not exceed the ICNIRP exposure limit for general public, but at mid-span it can be as high as 57.4 μT, which represents more than half of this limit. Towards the tower, it falls to only 14.85% of the limit.

Table 7 Input data for the 400 kV single-circuit OHVPL using towers of PAS 400.102 type

Phase conductor	i	d_i [m]	h_i [m]	\underline{U}_i [kV]	\underline{I}_i [A]
A	1	-11.50	h_g	231 ∠ 0°	975 ∠ 0°
	2	-11.10	h_g	231 ∠ 0°	975 ∠ 0°
B	3	-0.20	h_g	231 ∠ -120°	975 ∠ -120°
	4	0.20	h_g	231 ∠ -120°	975 ∠ -120°
C	5	11.10	h_g	231 ∠ 120°	975 ∠ 120°
	6	11.50	h_g	231 ∠ 120°	975 ∠ 120°

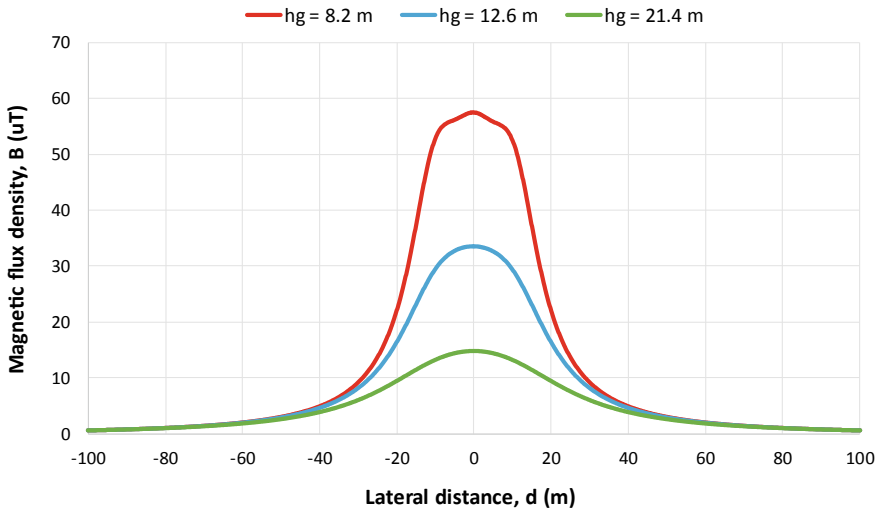


Fig. 24 RMS mag-netic flux density profiles for the 400 kV OHVPL, for various ground clearances

Table 8 Typical magnetic field levels from the 400 kV OHVPL ($h_g = 12.6$ m, $I = 450$ A)

B [μ T], at various lateral distances

<i>Maximum beneath line</i>	<i>25 m</i>	<i>37.5 m</i>	<i>50 m</i>	<i>100 m</i>
7.73	2.64	1.22	0.69	0.16

Once again, Table 8 gives magnetic field levels at various distances from the OHVPL centerline for the average clearance $h_g = 12.6$ m and a (normal) loading of 450 A. As it can easily be observed, the magnetic flux density at the OHVPL centerline is 7.73 μ T, while at the edge of the OHVPL corridor—37.5 m from the centerline [41]—it decreases to only 1.22 μ T. The critical value of 0.4 μ T is reached at a lateral distance of about 65.1 m.

b. Electric field distribution

The RMS electric field strength distribution at the height $h = 1$ m is illustrated in Fig. 25. This time, the electric field at mid-span ($h_g = 8.2$ m) is about two times higher than the ICNIRP exposure limit for general public, namely 9145.3 V/m. Towards the tower ($h_g = 21.4$ m), the electric field strength falls to 1970.9 V/m (39.41% of the limit), but, as the ground clearance increases, the maximum field levels slightly move outside the line (for $h_g = 21.4$ m, the maximum field strength is recorded at a distance of 16 m from the OHVPL centerline).

Finally, Table 9 gives electric field levels for the average clearance $h_g = 12.6$ m. The electric field strength beneath the line reaches 4752 V/m, decreasing to 776.4 V/m at the corridor edge (37.5 m from the OHVPL centerline) and to 340.2 V/m at

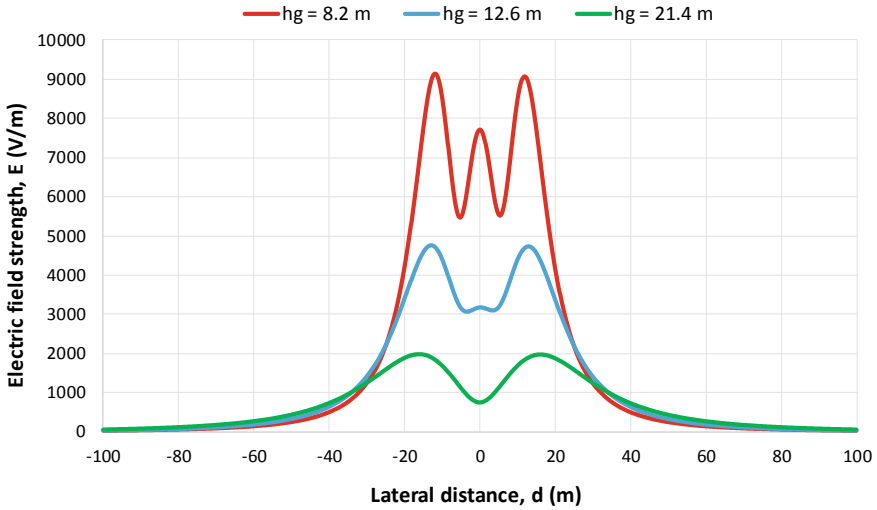


Fig. 25 RMS electric field strength profiles for the 400 kV OHVPL, for various ground clearances

Table 9 Typical electric field levels from the 400 kV OHVPL ($h_g = 12.6$ m)

E [V/m], at various lateral distances				
Maximum beneath line	25 m	37.5 m	50 m	100 m
4752	2212.7	776.4	340.2	44.1

50 m from the OHVPL centerline. At 100 m lateral distance, the electric field drops drastically, to only 44.1 V/m.

c. Alternative computation approach

All computations performed above assume that each sub-conductor of the considered 400 kV single-circuit OHVPL is modeled separately. However, this model can be simplified by replacing each of the three bundled conductors with an equivalent conductor of radius R_{eq} , given by [42]:

$$R_{eq} = \sqrt[N]{R \cdot d^{(N-1)}}, \tag{3}$$

where N stands for the number of sub-conductors in bundle, R represents the radius of a sub-conductor and d is the separation distance between sub-conductors. Equation (3) is applicable for up to three conductors per bundle, in our case leading to $R_{eq} = 76.485$ mm.

Figure 26 compares RMS magnetic flux density profiles computed with ANSYS Maxwell 2D by both approaches, as well as with PowerMAG software, which makes

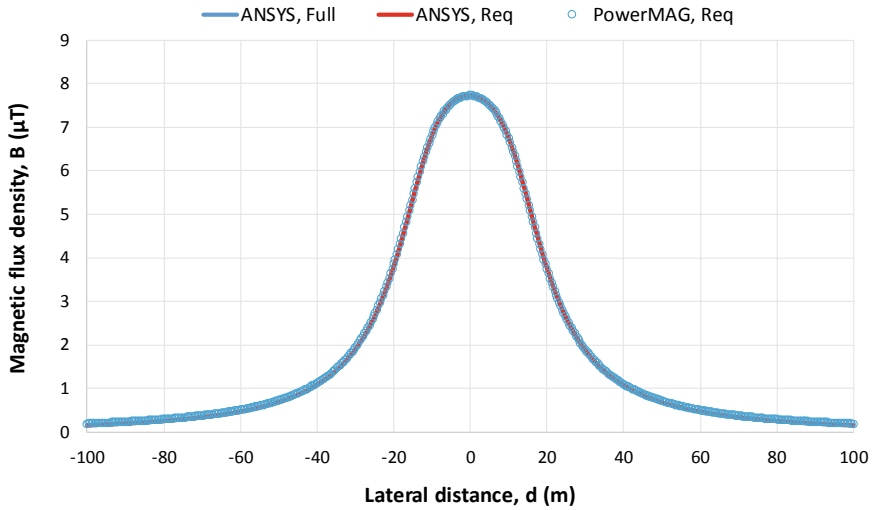


Fig. 26 Comparison between RMS magnetic flux density profiles obtained by the two approaches with ANSYS Maxwell 2D and PowerMAG software ($h_g = 12.6$ m, $I = 450$ A)

use of equivalent conductor model. As it can be observed, there is an excellent agreement between the three magnetic field profiles.

Similarly, Fig. 27 compares RMS electric field strength profiles computed with ANSYS Maxwell 2D by both approaches, as well as with PowerELT software, which

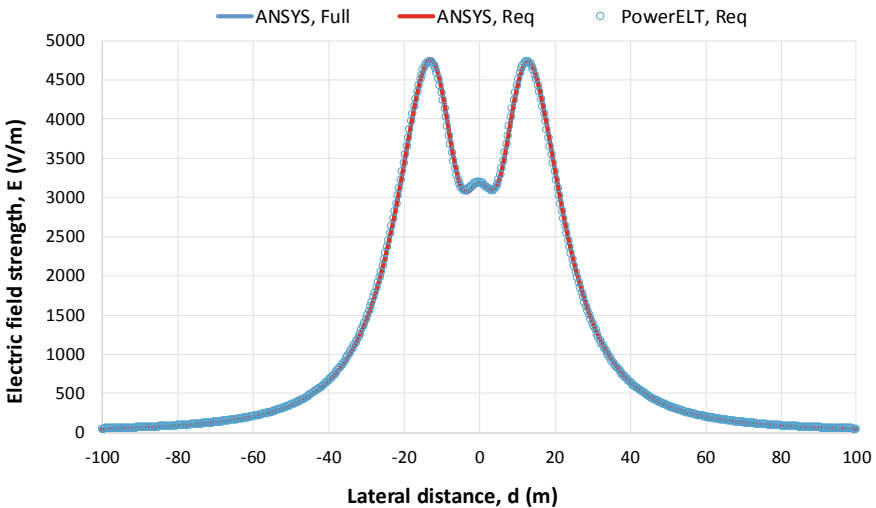


Fig. 27 Comparison between RMS electric field strength profiles obtained by the two approaches with ANSYS Maxwell 2D and PowerELT software ($h_g = 12.6$ m)

also makes use of equivalent conductor model. And this time, an excellent agreement between the three electric field profiles can be observed.

4 Conclusions

This chapter has been devoted to computing and analyzing ELF electric and magnetic fields emitted by typical configurations of OHVPLs used in Romania. All computations have been conducted using a 2D ANSYS Maxwell finite element model, strictly verified by quasi-static analytical methods. According to the obtained results, the highest exposure levels to ELF electric fields are associated with the 400 kV OHVPLs, directly beneath the line approaching the double of the ICNIRP limit for general public. As for ELF magnetic fields, the highest exposure levels are also associated with the 400 kV OHVPLs, but they are approaching only 60% of the ICNIRP limit. At the edge of the line corridor, the typical ELF electric and magnetic fields originating on the investigated OHVPLs are well below the specified limits, regardless the nominal voltage of the line. The computed ELF-EMF exposure levels are in line with those determined for similar OHVPLs in other countries.

References

1. Ahlbom A, Day N, Feychting M et al (2000) A pooled analysis of magnetic fields and childhood leukaemia. *Br J Cancer* 83:692–698
2. Greenland S, Sheppard AR, Kaune WT et al (2000) A pooled analysis of magnetic fields, wire codes, and childhood leukemia. *Child Leuk-EMF Study Group Epidemiol* 11:624–634
3. IARC Working Group (2002) IARC monographs on the evaluation of carcinogenic risks to humans series. Non-ionizing radiation, Part 1: static and extremely low-frequency (ELF) electric and magnetic fields, vol. 80. IARC Press, Lyon. <https://monographs.iarc.fr/ENG/Monographs/vol80/mono80.pdf>. Last accessed 28 Sept 2019
4. ICNIRP (1998) Guidelines for limiting exposure to time-varying electric, magnetic and electromagnetic fields (up to 300 GHz). *Health Phys* 74:494–522
5. IEEE (2002) C95.6-2002 IEEE standard for safety levels with respect to human exposure to electromagnetic fields 0 to 3 kHz, New York
6. Porsius JT, Claassen L, Smid T, et al (2014) Health responses to a new high-voltage power line route: design of a quasi-experimental prospective field study in the Netherlands. *BMC Public Health* 14(237):1–12. <https://www.ncbi.nlm.nih.gov/pmc/articles/PMC3975333/#B8>. Last accessed 28 Sept 2019
7. Porsius JT, Claassen L, Smid T et al (2015) Symptom reporting after the introduction of a new high-voltage power line: a prospective field study. *Environ Res* 138:112–117
8. Sahbudin RKZ, Fauzi SA, Hitam S et al (2010) Investigation of electrical potential and electromagnetic field for overhead high voltage power lines in Malaysia. *J Appl Sci* 10(22):2862–2868
9. Elhabashi SM, Ehtaiba JE (2007) Electric fields intensity around the new 400 kV power transmission lines in libya. In: Proceedings of the 6th WSEAS international conference on circuits, systems, electronics, control and signal processing, Cairo, 29–31 Dec 2007, pp 390–398
10. EMFs.info (2019) Factors affecting the field from a power line. <https://www.emfs.info/sources/overhead/factors/>. Last accessed 28 Sept 2019

11. Vornicu S, Lunca E, Salceanu A (2019) ANSYS maxwell finite element model for 2D computation of the magnetic field generated by overhead high-voltage power lines. In: Proceedings of the 12th international conference and exhibition on electromechanical and energy systems (SIELMEN 2019), Chisinau, 10–11 Oct 2019, pp 382–385
12. Fuchs E, Masoum MAS (2008) Power quality in power systems and electrical machines. Elsevier Academic Press, Burlington
13. Olsen RG, Deno D, Baishiki RS et al (1988) Magnetic fields from electric power lines: theory and comparison to measurements. *IEEE Trans Power Deliv* 3(4):2127–2136
14. Vujević S, Lovrić T, Modrić T (2011) 2D computation and measurement of electric and magnetic fields of overhead electric power lines. In: Proceedings of the joint 3rd international workshop on nonlinear dynamics and synchronization (INDS'11) & 16th international symposium on theoretical electrical engineering (ISTET'11), Klagenfurt, 25–27 July 2011, pp 1–6
15. Kokoruš M, et al (2014) Analysis of the possible solutions for the reduction of electric and magnetic fields near 400 kV overhead transmission lines. In: Passerini G, Brebbia CA (eds) Environmental impact II. 2nd international conference on environmental and economic impact on sustainable development, Ancona, May 2014. WIT transactions on ecology and the environment, vol. 181. WIT Press, Southampton, p 225
16. Ellithy K, Al-Suwaidi S, Elsayed H (2011) Measuring human exposure to magnetic fields near EHV 400 kV GIS substation and power lines in state of qatar. In: Proceedings of the north American power symposium (NAPS 2011). Boston, 4–6 Aug 2011, pp 1–6
17. Medved D, Mišenčik L, Kolcun M, et al (2015) Measuring of magnetic field around power lines. In: Proceedings of the 8th international scientific symposium ELEKTROENERGETIKA 2015. Stará Lesná, 16–18 Sept 2015, pp 148–151
18. Vergara XP, Kavet R, Crespi CM et al (2015) Estimating magnetic fields of homes near transmission lines in the California power line study. *Environ Res* 140:514–523
19. Tourab W, Babouri A (2016) Measurement and modeling of personal exposure to the electric and magnetic fields in the vicinity of high voltage power lines. *Saf Health Work* 7(2):102–110
20. Filippopoulos G, Tsanakas DK (2005) Analytical calculation of the magnetic field produced by electric power lines. *IEEE Trans Power Deliv* 20(2):1474–1482
21. Moro F, Turri R (2008) Fast analytical computation of power-line magnetic fields by complex vector method. *IEEE Trans Power Deliv* 23(2):1042–1048
22. Ztoupis IN, Gonos IF, Stathopoulos IA (2013) Calculation of power frequency fields from high voltage overhead lines in residential areas. In: Proceedings of the 18th international symposium on high voltage engineering. Seoul, 25–30 Aug 2013, pp 61–66
23. Milutinov M, Juhas A, Prša M (2007) Electric field strength and polarization of multi three-phase power lines. In: Proceedings of the 8th international conference on applied electromagnetics. Niš, 3–5 Sept 2007, pp 1–4
24. Milutinov M, Juhas A, Prša M (2009) Electromagnetic field underneath overhead high voltage power line. In: Proceedings of the 4th international conference on engineering technologies. Novi Sad, 28–30 April 2009, pp 1–5
25. Al Salameh MSH, Hassouna MAS (2010) Arranging overhead power line conductors using swarm intelligence technique to minimize electromagnetic fields. *Prog Electromagn Res B* 26:213–236
26. Gouda OE, Amer GM, Salem WA (2009) Computational aspects of electromagnetic fields near H.V. Transmission lines. *Energy Power Eng* 1(2):65–71
27. Lunca E, Istrate M, Salceanu A et al (2012) Computation of the magnetic field exposure from 110 kV overhead power lines. In: Proceedings of the 7th international conference on electrical and power engineering. Iasi, 25–27 Oct 2012, pp 628–631
28. Lunca E, Ursache S, Salceanu A (2018) Computation and analysis of the extremely low frequency electric and magnetic fields generated by two designs of 400 kV overhead transmission lines. *Measurement* 124:197–204
29. Razavipour SS, Jahangiri M, Sadeghipoor H (2012) Electrical field around the overhead transmission lines. *World Acad Sci Eng Technol* 6(2):168–171

30. Lunca E, Istrate M, Salceanu A (2013) Comparative analysis of the extremely low-frequency magnetic field exposure from overhead power lines. *Environ Eng Manag J* 12(6):1145–1152
31. Ali Rachedi B, Babouri A, Berrouk F (2014) A study of electromagnetic field generated by high voltage lines using COMSOL MULTIPHYSICS. In: Proceedings of the 2014 international conference on electrical sciences and technologies in Maghreb. Tunis, 3–6 Nov 2014, pp 1–5
32. Salceanu A, Lunca E, Paulet M (2017) Affordable evaluation of low frequency electric fields from the standpoint of directive 2013/35/EU. *ACTA IMEKO* 6(4):37–45
33. Lunca E, Vornicu S, Salceanu A et al (2018) 2D Finite element model for computing the electric field strength-rms generated by overhead power lines. *J Phys Conf Ser* 1065:1–4
34. EU (1999) 1999/519/EC: Council recommendation of 12 July 1999 on the limitation of exposure of the general public to electromagnetic fields (0 Hz to 300 GHz). <https://publications.europa.eu/en/publication-detail/-/publication/9509b04f-1df0-4221-bfa2-c7af77975556/language-en>. Last accessed 28 Sept 2019
35. Braicu SF, et al (2017) Evaluation of the electric and magnetic field near high voltage power lines. In: Vlad S, Roman NM (eds) MEDITECH 2016. 5th international conference on advancements of medicine and health care through technology. Cluj-Napoca, 2016. IFMBE proceedings, vol. 59, Springer International Publishing, p 141
36. Ghani SA, Ahmad Khair MS, Chairul IS, et al (2014) Study of magnetic fields produced by transmission line tower using finite element method (FEM). In: Proceedings of the 2nd international conference on technology, informatics, management, engineering & environment. Bandung, 19–21 Aug 2014, pp 64–68
37. EMFs.info (2019) Phasing—how the phasing affects the field produced by an overhead line. <https://www.emfs.info/sources/overhead/factors/phasing/>. Last accessed 28 Sept 2019
38. Ponnle AA, Adedeji KB, Abe BT et al (2017) Variation in phase shift of phase arrangements on magnetic field underneath overhead double-circuit HVTLs: field distribution and polarization study. *Prog Electromagn Res M* 56:157–167
39. Lunca E, Ursache S, Salceanu A (2017) Characterization of the electric and magnetic field exposure from a 400 kV overhead power transmission line in Romania. In: Proceedings of the 22nd IMEKO TC4 international symposium and 20th international workshop on ADC modelling and testing. Iasi, 14–15 Sept 2017, pp 239–243
40. Transelectrica (2019) Power transmission grid. <https://www.transelectrica.ro/en/web/tel/date-generale-management>. Last accessed 28 Sept 2019
41. ANRE (2007) Technical norm regarding the delimitation of the protection and safety zones associated with energy capacities—Revision I of 09 March 2007
42. Grigsby LL (2012) *Electric power generation, transmission, and distribution*, 3rd edn. CRC Press, Boca Raton